Supporting Information

Amplified Spontaneous Emission Dependence on Temperature-Induced Crystalline Phase Transition in a Solution Processed $MAPbBr_3$ Thin Film

Maria Luisa De Giorgi[1*], Titti Lippolis[1], Nur Fadilah Jamaludin[2], Cesare Soci[3], Annalisa Bruno[2], Marco Anni[1]

[1]*Dipartimento di Matematica e Fisica "Ennio De Giorgi", Università of Salento, 73100 Lecce, Italy*

[2]*Energy Research Institute @ NTU (ERI@N), Nanyang Technological University, 637553, Singapore*

[3]*Division of Physics and Applied Physics, School of Physical and Mathematical Sciences, Nanyang Technological University, 637371, Singapore*

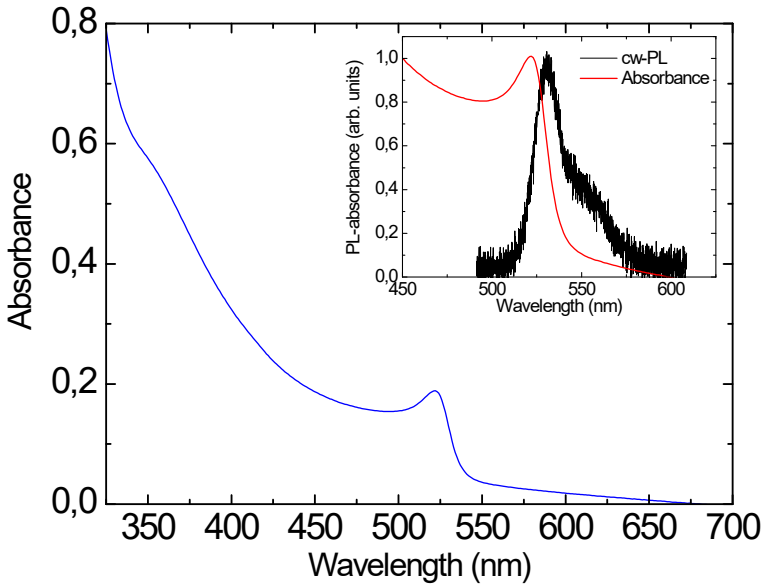

Figure S1: Absorbance spectrum of the film. Inset: lineshape comparison between the absorbance and the PL spectrum (the spectra are normalized to 1 on the peak).

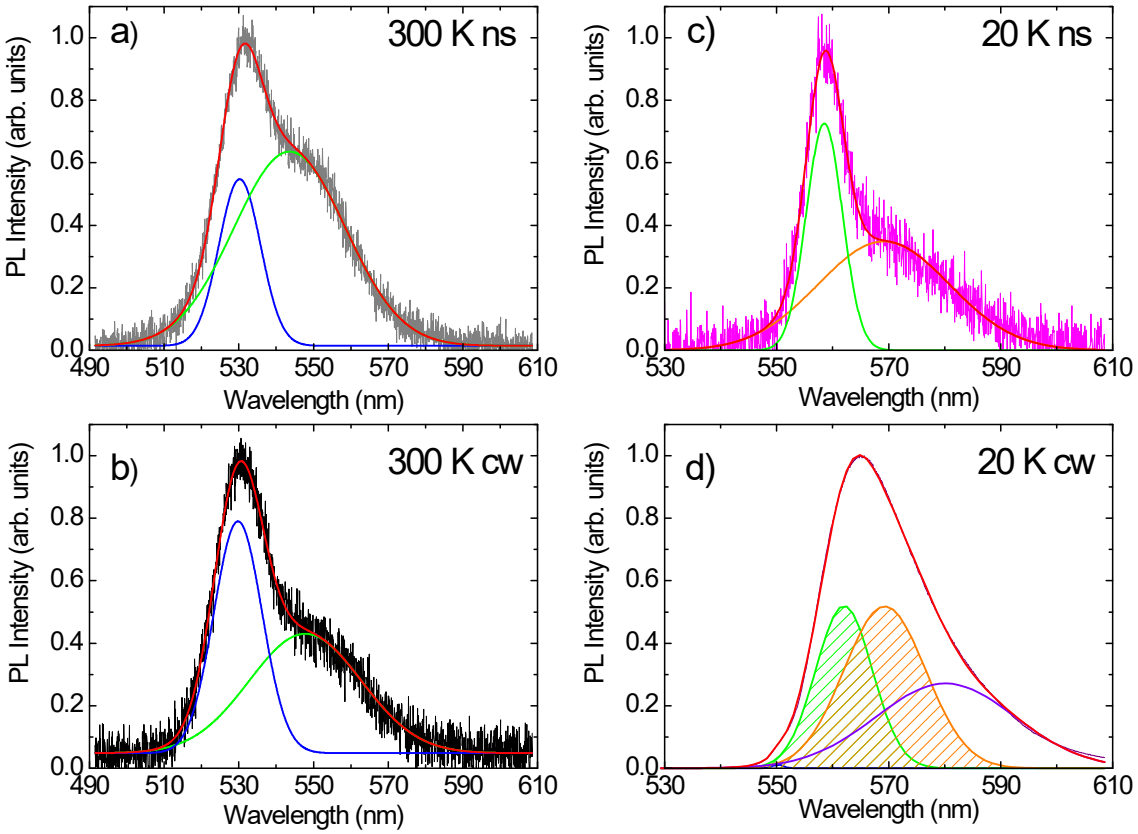

Figure S2: a): PL spectrum acquired at 300 K under nanosecond pumping, below the ASE threshold, and the two Gaussian bands used to reproduce it. The blue peak is relative to FE emission, while the green one to BE emission. b): PL spectrum at 300 K under continuous wave excitation, evidencing the presence of FE and BE emission, similar to what observed under nanosecond pumping. c): PL spectrum acquired at 20K, below the ASE threshold, and the two Gaussian bands used to reproduce it. The green peak is relative to BE emission, while the red one is a new peak only visible below 100 K. d) PL spectrum at 20 K under continuous wave excitation, evidencing a clearly different line-shape with respect to the nanosecond pumping spectrum, and the presence of a further emission band at high wavelength (blue peak). The shaded peaks are the two peaks visible under nanosecond pumping.

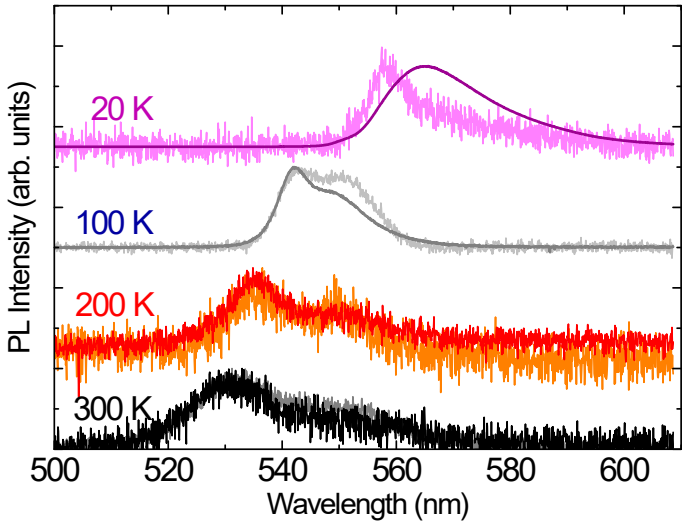

Figure S3: lineshape comparison between the PL spectra under cw-pumping (darker lines) and under nanosecond pumping below threshold.

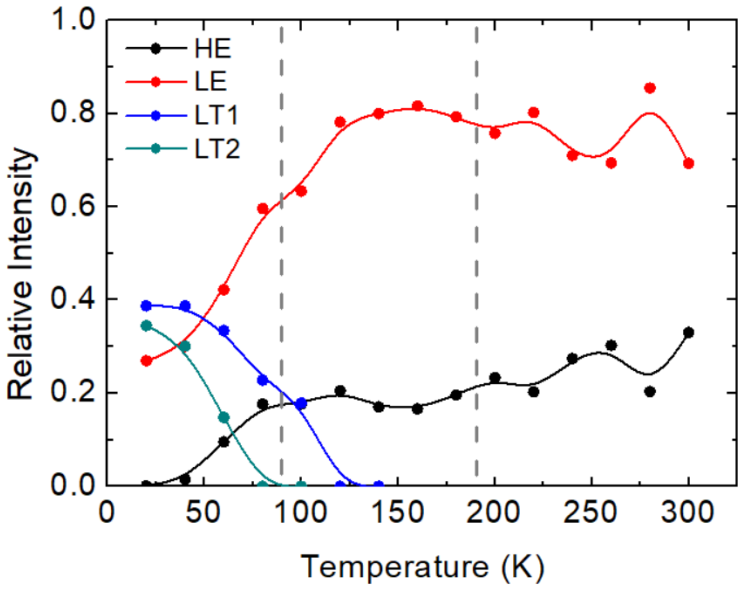

Figure S4: temperature dependence of the relative intensity of the various peaks contributing to the cw-PL spectra.

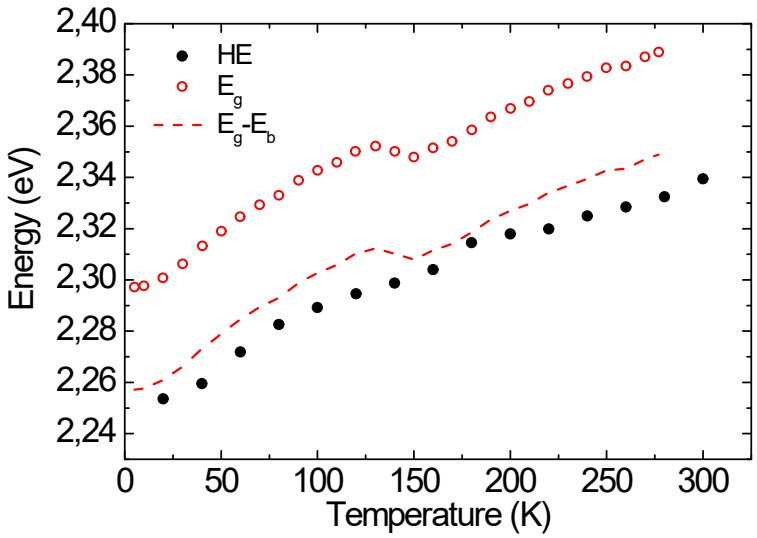

Figure S5: temperature dependence of the HE peak energy, compared with the energy gap (E_g), and the estimated FE emission, obtained by subtracting the exciton binding energy (E_b) to the E_g values, by using the results of reference [48].

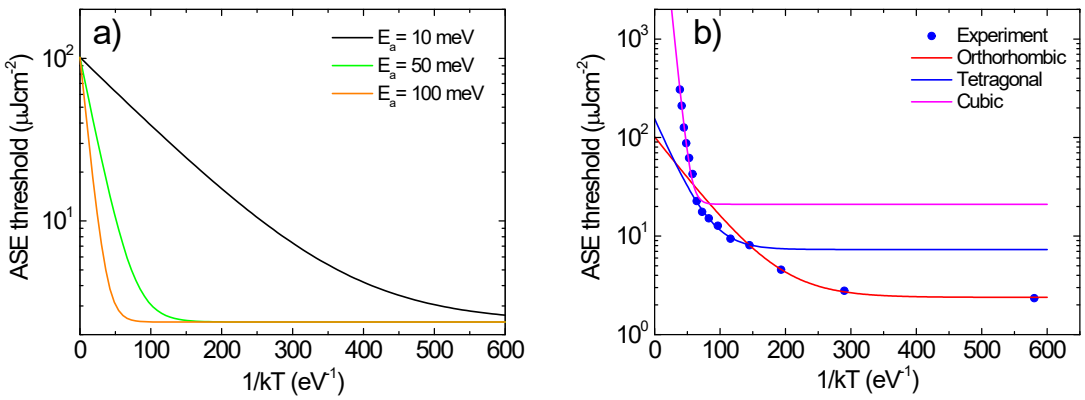

Figure S6: a): simulated ASE threshold dependence as a function of the activation energy (for D_0 and D_1 fixed to the best fit values of the orthorhombic phase). It is evident that the activation energy increase leads to an increase of the temperature range in which the threshold increases, but also to a steeper growth. b): simulated ASE threshold temperature dependence for the three phases in the whole temperature range, allowing an ideal comparison in case of stable phases at every temperature.

Evaluation of laser-induced heating effects

To evaluate the sample heating effect under laser excitation, the analysis starts with the examination of the power spectra acquired at four different temperatures (20, 100, 200, and 300 K). As the excitation energy density increases, if laser-induced heating were significant, one would expect a blue-shift of ASE peak, as observed when the sample temperature is increased (as reported in Figure 2). However, no peak shift is observed at 20 K up to the maximum explored energy density, while a very small red-shift of 0.5 nm, 0.8 nm and 1.0 nm is observed at 100 K, 200 K and 300 K, respectively. We can thus conclude that our spectra do not show the variations expected for appreciable sample heating during the measurements, reasonably due to the limited exposure time of the sample in each measurement (1 second), and to the high heat capacity of the cryostat cold-finger, that is in thermal contact with the sample.

Once excluded sample heating up to an excitation density of 0.9 mJ/cm^2 (the highest in the spectra measurement at room temperature, and the fixed value for the ASE spectra measurements as a function of the temperature), we can also exclude any heating effect in the ASE threshold values, as these measurements are done by progressively increasing the excitation density, up to the appearance of the ASE band. The sample is then exposed to excitation densities below the threshold, thus at excitations density well below 0.9 mJ/cm^2 (from 3 times lower at room temperature to about 500 times lower at 20 K). This conclusion is also confirmed by the good correspondence between the temperatures at which the discontinuity of the ASE temperature variation is observed, with the discontinuities observed in the PL temperature dependence under CW excitation. The cw measurements are performed at an excitation power density of approximately 0.3 W/cm^2—more than four orders of magnitude lower than the excitation power densities corresponding to an excitation energy density of just 1 $\mu J/cm^2$ under nanosecond pumping.

In conclusion, we can exclude any significant heating effect of the sample induced by laser irradiation, and we are confident that the possible influence on the emission properties (PL and ASE), on the ASE threshold, and on the phase transitions can be regarded as negligible.

Defect Density Estimation

Concerning defects density generating the emission from LT1 and LT2, it could be estimated from the excitation density dependence of the LT1 peak at 20 K, and from the absence of LT2 emission at any excitation density.

As the defects density is typically much lower than the intrinsic states one, the defect related emission is characterized by an intensity saturation for high enough excitation density. We thus investigated

the excitation density dependence of the LT1 peak at 20 K, under nanosecond pumping, after converting the excitation density in pump photons volumetric density.

Considering that the excitation is performed with a laser at 337 nm, it is straightforward to demonstrate that an excitation density of 1 μJ/cm^2 corresponds to a pump photon density in the film of 1.7 10^{17} cm^{-3}.

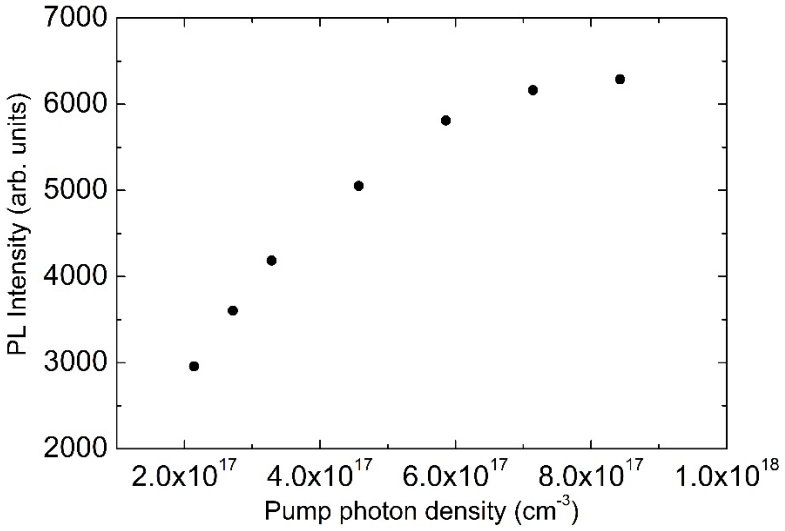

Figure S7: photon density dependence of PL intensity under ns-pumping

The results obtained (as reported in Figure S7) clearly evidence a progressive saturation, that is basically complete at about 8 10^{17} cm^{-3}. This value would correspond to the defect density, if all the absorbed photons would lead only to defect emission. However, in our case, in the saturation pumping range of the LT1 peak, we observe a much stronger intrinsic emission, demonstrating that most of the excitation density generates excitons, without populating the states generating the LT1 peak. Thus, the value of 8 10^{17} cm^{-3} can be taken as an upper limit for the defect states related to the LT1 peak.

Concerning the defects related to LT2, we observe that no measurable emission contribution from these defects is observed already at the lowest excitation density corresponding to a photon density of 2 10^{17} cm^{-3}, showing that defects saturation takes place at even lower excitation densities. The photon density of 2 10^{17} cm^{-3} can thus be taken as an upper limit for the defect density.

The obtained values are quantitatively comparable with the surface defects density of both $MAPbBr_3$ single crystals [ref 62 of the manuscript] and of $MAPBI_3$ polycrystalline thin films [ref 72 of the manuscript].

Effect of Temperature-Induced Changes in Refractive Index and Crystal Size

To evaluate the possible influence of the temperature dependence of the refractive index, we note that, as reported in [ref 1], the temperature-induced variation of the refractive index of $MAPbBr_3$ within the ASE emission range is extremely small (well below 0.1).

To probe the effects of this variation on the film waveguiding properties, we simulated the effect on the TE_0 guided mode of refractive index variation, assuming for safety an overestimated n variation of 0.1, from 2.0 to 2.1 as the temperature decreases from 300 to 20 K.

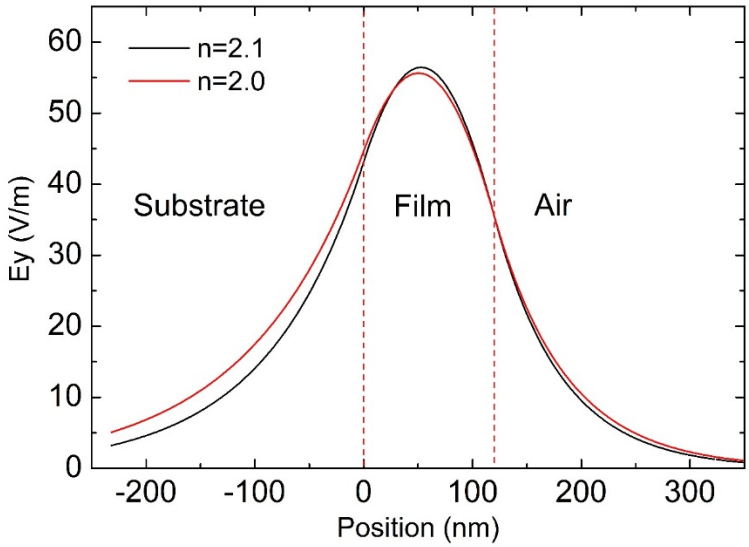

Figure S8: Simulation of the TE_0 mode at 300 K (red line) and at 20 K (black line) evidencing the very small variation induced by the refractive index variation.

As evident from the results, the refractive index variation leads to a very small variation of the mode profile, and to a corresponding small variation of the mode confinement (see ref 2) from 48.3% at 300 K to 51.5% at 20 K. A relative variation of mode confinement of just 6% is clearly not compatible with a threshold variation of more than 100 times, allowing us to rule out any relevant effect of the temperature variation of the refractive index.

We also considered the possible variation in scattering due to thermal expansion. As the temperature increases, an enlargement of the crystalline grains would reduce the number of scattering events along the pump stripe, thus leading to lower losses, and thus providing a contribution to an ASE threshold decrease. However, a strong rise in the threshold is experimentally observed. In addition, also in this case the absolute value of thermal expansion between 20 K and 300 K is about 1.5% (see ref 3), allowing us to estimate low scattering variation across the investigated temperature range.

Physical Interpretation of Fitting Parameters for the Cubic Phase

Concerning the cubic phase, which is the one showing ASE at room temperature, we observe a much higher activation energy of the non radiative process, as well as clearly increased values of D_0, D_1 and of their ratio.

Before drawing any conclusion, it is preliminarily useful to check the physical reasonability of these results. First, we observe that the obtained value of the activation energy is very similar to the one found for the activation energy of the PL quenching in [ref. 47 of manuscript], in the same temperature range. Concerning instead the increased values of D_0 and D_1, the possible contributions are an increase of the α/σ ratio, a decrease of the temperature independent lifetime τ_0 and a decrease of the defects coupling lifetime τ_{0nr}. However, a D_0 and D_1 variation only due to the α/σ ratio variation would lead to an identical relative variation of both parameters, without any variation of their ratio.

In our case we instead observe a clear difference in the relative increase of D_0 (about 3 times) and D_1 (about 880 times), with a corresponding variation of their ratio of about 250 times. This result clearly suggests that the variation of the D_0 and D_1 parameters is a signature of variation of the lifetimes.

This outcome is anyway consistent with previous experiments on $MAPbBr_3$. In particular, in [ref 43 in the manuscript] the authors observe a lifetime decrease of the exciton emission (typically related to the τ_0 lifetime), and an increased contribution to the PL relaxation of traps emission, consistent with the increase of the trapping rate, included in our model in the thermally activated term. Similar results were also obtained in [ref 45 in the manuscript], in which evidence of traps emission are obtained only in the cubic phase, evidencing an increasing trapping in the cubic phase with respect to the tetragonal one.

This result is perfectly consistent with the observed increase of the exciton coupling constant with the temperature dependent decay channel, given by $1/\tau_{0nr}$.

We can thus conclude that the observed huge increase of the best fit parameters in the cubic phase is not a fitting artefact.

[1] H. Laysandra,Y.-C. Chao, H.-L. Liu, *J. Phys. Chem. C* 2022, **126**, 797

[2] M. Anni, A. Perulli, G. Monti, *J. Appl. Phys*. 2012, **111**, 093109

[3] M. Keshavarz, M. Ottesen, S. Wiedmann, M. Wharmby, R. Küchler, H.Yuan, E. Debroye, J. A. Steele, J. Martens, N. E. Hussey, M. Bremholm, M. B. J. Roeffaers, J. Hofkens, *Adv. Mater.* 31, **2019**, 1900521